Performance characterization of an integrated ultrasound, photoacoustic, and thermoacoustic imaging system

Haixin Ke
Todd N. Erpelding
Ladislav Jankovic
Changjun Liu
Lihong V. Wang

Performance characterization of an integrated ultrasound, photoacoustic, and thermoacoustic imaging system

Haixin Ke,a Todd N. Erpelding,b Ladislav Jankovic,b Changjun Liu,a,c and Lihong V. Wang
aWashington University, Department of Biomedical Engineering, Optical Imaging Laboratory, St. Louis, Missouri
bPhilips Research North America, Briarcliff Manor, New York
cSichuan University, School of Electronics and Information Engineering, Chengdu, China

Abstract. We developed a novel trimodality system for human breast imaging by integrating photoacoustic (PA) and thermoacoustic (TA) imaging techniques into a modified commercial ultrasound scanner. Because light was delivered with an optical assembly placed within the microwave antenna, no mechanical switching between the microwave and laser sources was needed. Laser and microwave excitation pulses were interleaved to enable PA and TA data acquisition in parallel at a rate of 10 frames per second. A tube (7 mm inner diameter) filled with oxygenated bovine blood or 30 mM methylene blue dye was successfully detected in PA images in chicken breast tissue at depths of 6.6 and 8.4 cm, respectively, for the first time. The SNRs at these depths reached ∼24 and ∼15 dB, respectively, by averaging 200 signal acquisitions. Similarly, a tube (13 mm inner diameter) filled with saline solution (0.9%) at a depth of 4.4 cm in porcine fat tissue was successfully detected in TA images. The PA axial, lateral, and elevational resolutions were 640 μm, 720 μm, and 3.5 mm, respectively, suitable for breast cancer imaging. A PA noise-equivalent sensitivity to methylene blue solution of 260 nM was achieved in chicken tissue at a depth of 3.4 cm. © 2012 Society of Photo-Optical Instrumentation Engineers (SPIE). [DOI: 10.1117/1.JBO.17.5.056010]

1 Introduction

Ultrasound (US) imaging is widely used for clinical diagnostic imaging, but its application in cancer detection is limited by poor sensitivity. Photoacoustic (PA) tomography (PAT) and thermoacoustic (TA) tomography (TAT) are novel hybrid imaging techniques that achieve both high ultrasonic resolution and high contrast owing to light or microwave/radio-frequency (RF) absorption.[1,2] Photoacoustic and thermoacoustic effects are based on the generation of pressure waves upon absorption of electromagnetic energy.[3] Absorbed energy is converted into heat, which launches a pressure wave via thermoelastic expansion. In PAT, biological tissues are usually irradiated by a pulsed laser. When the excitation laser is replaced by microwave or RF sources, the technique is called TAT.[4–6] PA or TA image contrasts reflect the absorbed optical or RF energy within the sample, respectively. The absorption reveals optical or dielectric properties of the tissue that are closely related to its physiological and pathological state.[1,7] PAT/TAT overcomes the disadvantages of pure optical or microwave/RF imaging, such as shallow penetration depth or poor spatial resolution, and the disadvantages of pure ultrasonic imaging, such as poor soft-tissue contrast and speckle.

PAT and TAT techniques have been widely studied for biomedical applications, including brain structural and functional imaging, blood oxygenation and hemoglobin monitoring, and imaging of tumor angiogenesis.[8–13] Recently, investigations have sought to improve PAT/TAT performance.[14–17] The results showed that PAT/TAT was capable of high-resolution structural, functional, and molecular imaging that was free of speckle artifacts. Combinations of PAT/TAT or PAT/US were investigated for breast cancer and sentinel lymph node imaging.[1,3,18–21] A coregistered PA, TA, and US system has been constructed for small-animal imaging,[22] where different detectors were used for PA/TA and US data.

We successfully integrated all three modalities (US/PA/TA) into one system based on a modified clinical US imaging scanner. Figure 1(a) shows a photograph of the integrated clinical system. Patients lie in the prone position on a bed with a large round opening. The breast is positioned through the round opening onto a transparent plate. Laser and microwave are delivered from below the patient, and coregistered US/PAT/TAT images can be acquired. The complementary contrast mechanisms provided by an integrated US/TAT/PAT system could provide a novel method to monitor and predict response to breast cancer therapies.[8,23,24] The functional contrast mechanisms provided by TAT/PAT have the potential to assess therapeutic response at an earlier time than the morphological contrast mechanisms detected by conventional anatomical imaging modalities. We tested our system using embedded objects with known optical absorption characteristics in *ex vivo* tissue. In this article, we present results of the system performance in terms of resolution, sensitivity, and penetration depth.

2 Materials and Methods

2.1 PA/TA/US System

Figure 1(b) shows a block diagram of the trimodality imaging system that we developed by modifying a clinical US imaging

Address all correspondence to: Lihong V. Wang, Washington University, Department of Biomedical Engineering, Optical Imaging Laboratory, St. Louis, Missouri. Tel.: +314 9356152; Fax: +314 9357448; E-mail: lhwang@wustl.edu
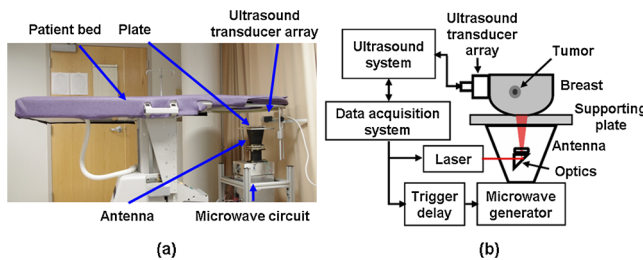
Fig. 1 The integrated trimodality imaging system. (a) Photograph showing the clinical setup. (b) Block diagram of the system.

scanner (iU22, Philips Healthcare). The system had four main components: a laser system, a microwave system, the modified clinical ultrasound scanner, and a custom-made data acquisition system. The commercial US scanner was modified to allow access to raw per-channel RF acoustic data, whereas all imaging capabilities of the scanner were retained.[19]

The laser system consisted of a tunable dye laser (Precision-Scan-P, Sirah) pumped by a Q-switched Nd:YAG laser (PRO-350-10, Newport). The chosen laser wavelength was 650 nm, where our laser system provides the highest power. The laser pulse width was 6.5 ns and the repetition rate was 10 Hz. Laser pulses were delivered by free-space optics to the opening of a horn antenna through a small hole on the narrow side wall and optically expanded to form a beam with a 1.6-cm radius at the antenna opening.

The microwave system generated 3.0-GHz microwave pulses with different pulse widths (0.16 to 1.2 μs) and repetition rates (<100 Hz) and directed the pulses toward the target through the horn antenna. For this study, the microwave pulse width was 0.6 μs and the repetition rate was 10 Hz. The peak power with 0.6-μs pulse width was 58 kW, which generated an average power density of 4.5 mW/cm^2 at the opening of the antenna, which is below the maximum permissible exposure limit set by the IEEE standard.[25] The size of the antenna opening was 11 by 7 cm. The hole in the antenna that allowed the laser beam to pass through was small compared to the microwave wavelength in air. The current distribution on the antenna, and therefore the electromagnetic field, was not significantly disturbed.

An US phased array probe (S5-1, Philips Healthcare) with 80 elements and a nominal frequency band of 1 to 5 MHz was used to acquire US, PA, and TA signals. Although this probe had a lower center frequency than typical breast imaging probes, it was well suited for detecting low-MHz-frequency, microwave-induced thermoacoustic signals. The custom-made data acquisition system controlled the triggering of all three modalities and collected raw data for image display and post-processing. PA and TA images were reconstructed using a delay-and-sum or Fourier beam-forming algorithm implemented in Matlab, generating cross-sectional B-mode images.[26] To improve the SNR, PA and TA acquisitions were repeated 200 times and raw data were averaged before image reconstruction.

2.2 PAT Experiments

Low-density polyethylene (LDPE) tubes filled with either oxygenated bovine blood or methylene blue dye (30 mM) were embedded in layers of chicken breast tissue and imaged using PA/US. In PA penetration-depth experiments, additional layers of chicken breast tissue were sequentially added to assess

the PA detection limits for the trimodality system. Methylene blue dye was used as a target for PAT because it is routinely used clinically during sentinel lymph node biopsy for axillary staging of breast cancer patients. In methylene blue detection-sensitivity experiments, an LDPE tube filled with methylene blue solution was buried within layers of chicken breast tissue at a fixed depth of ~3.5 cm, and the concentration of the solution was varied from 2 μM to 1 mM. In spatial resolution experiments, the PA resolutions were evaluated using black human hairs mounted on a plastic holder placed in a water tank.

2.3 TAT Experiments

LDPE tubes filled with saline solution (0.9%) diluted from phosphate saline buffer and embedded in porcine fat were imaged using TA/US. Saline solution was used for TAT because previous studies showed that TAT contrast between normal and tumor tissues was mainly due to the higher sodium and water content in tumors.[4,27] In TA penetration-depth experiments, additional layers of porcine fat were sequentially added to assess the TA detection limits for the trimodality system. The TA spatial resolutions were evaluated using a thin saline tube placed in a tank filled with mineral oil for TAT.

3 Results

3.1 Multimodality Phantom Imaging

A phantom test was conducted to validate and show the benefits of the trimodality system. The experiment setup is illustrated in Fig. 2(a). Three LDPE tubes filled with mineral oil, methylene blue (30 mM), or 0.9% saline solution were placed at the opening of the antenna. The US image, overlaid PA/US image, and overlaid TA/US image are shown in Fig. 2(b), 2(c), and 2(d), respectively. As expected, all three tubes were observed in the US image. Owing to the strong optical absorption of the dye at 650 nm, only the methylene blue tube was observed in the PA image. Both the methylene blue and saline solution tubes were observed in the TA image, but the signal from methylene blue was weaker than that from saline solution, as saline has stronger microwave absorption than methylene blue. Accurate coregistration of the tube locations was maintained in all three modalities, which was facilitated by using the same probe for detection of US, PA, and TA signals.

The tubes were identified in the images by the boundaries facing the ultrasound transducer. Because the low-frequency information in the acoustic signal was filtered by the transducer bandwidth, only the boundaries of the tubes were visible. Moreover, the transducer position was fixed and had a limited aperture for detection, leading to incomplete boundaries of the tubes in the images.[28]

The PA spatial resolutions of the trimodality imaging system were estimated using black human hairs immersed in a water tank. The PA axial and lateral resolutions were calculated from the FWHM widths in the cross-sectional hair images that were reconstructed using a Fourier transform algorithm. Figure 2(e) shows an image of the hairs placed at a depth of 2.7 cm. For PA elevational resolution, one hair was imaged in a longitudinal view (i.e., along the long axis of the transducer), and a 2-D maximum amplitude projection (MAP) image was created by scanning the transducer in the elevational direction. The PA elevational resolution was then measured from the FWHM of the hair signal in the resulting MAP image. Figure 2(f) shows
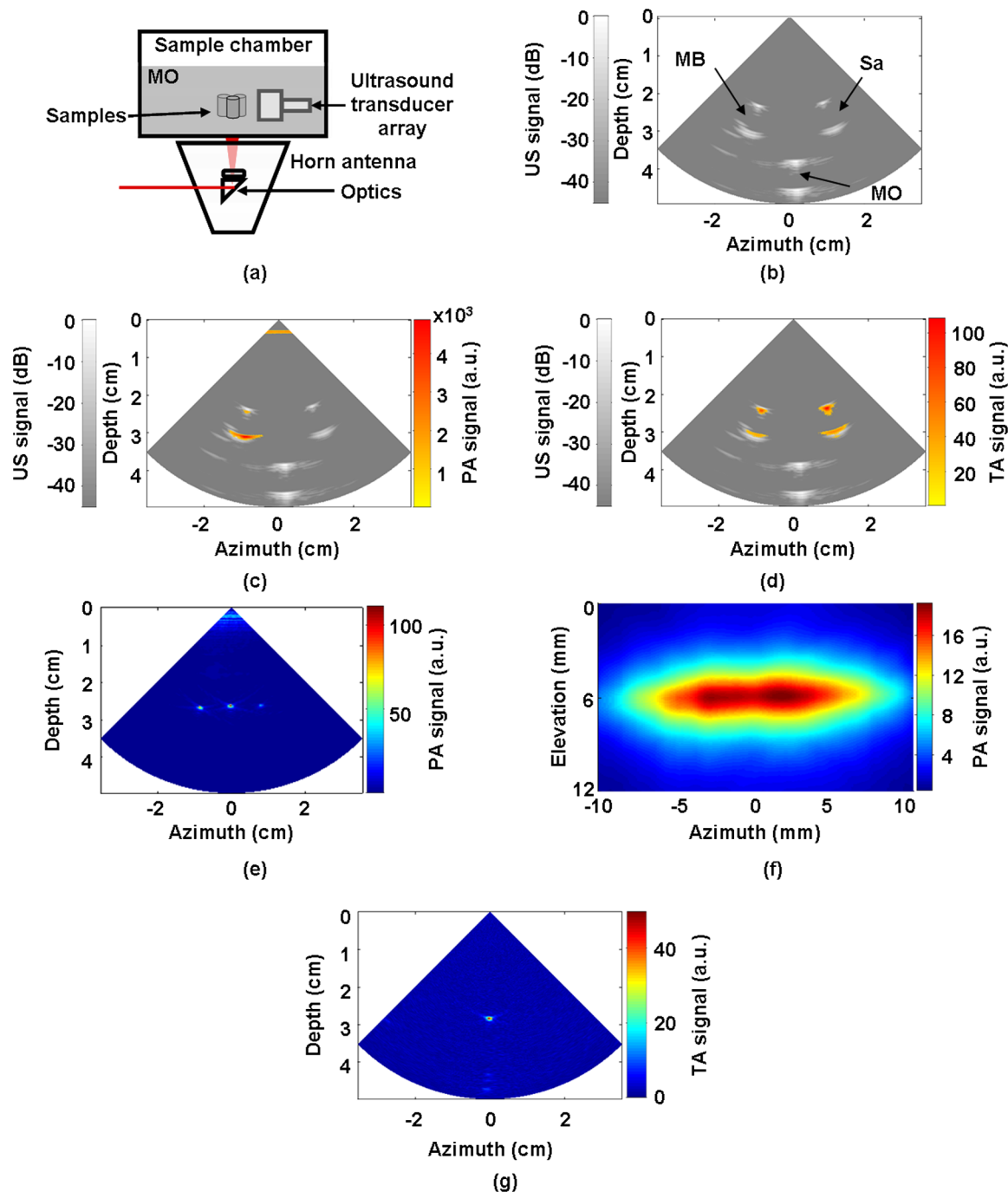
Fig. 2 PA/TA/US phantom images. (a) Diagram of the experimental setup imaging three tubes filled with different solutions. (b) US image showing all three tubes. MB, methylene blue; Sa, saline; MO, mineral oil. (c) Overlaid PA and US image. The PA image shows only the tube filled with MB. (d) Overlaid TA and US image. Both tubes filled with MB and Sa are shown in the TA image, and the Sa tube has stronger signal. (e) PA image showing the cross-section of three black human hairs. (f) MAP image of one hair in the *en face* view. (g) TA image showing the cross-section of a saline tube.

one such MAP image after interpolation in the width direction at a depth of 6 cm. The PA axial resolution, 640 μm, was nearly constant over the full range of depths. The PA lateral resolution ranged from 720 μm to 2 mm, and it increased with depth. The PA elevational resolution also varied with depth, and the best resolution was 3.5 mm. It is worth noting that in our PAT study, we used diffuse light to illuminate the sample, so the photoacoustic resolution of the system was determined by the ultrasound transducer. Scattering tissues such as human breast tissue will affect the SNR but not the resolution.
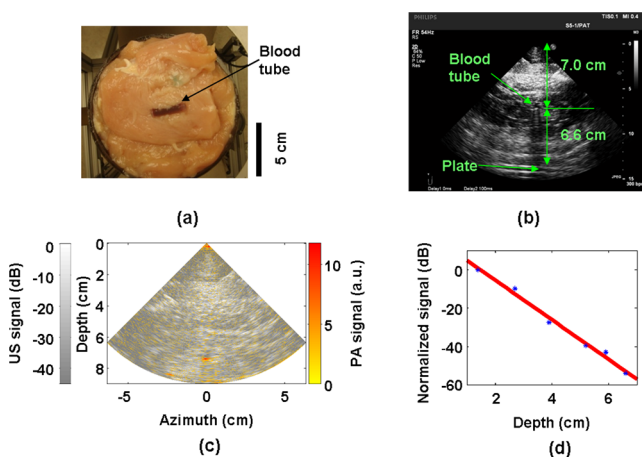
A similar resolution measurement was done for TAT using a thin tube (inner diameter ~0.3 mm) filled with 0.9% saline. TAT resolution depends on the microwave pulse width.[29,30] To minimize the effect of the microwave pulse width, we measured the temporal profile of the microwave pulse and used the Fourier deconvolution method described in Ref. 31. Figure 2(g) shows a TA image of the tube placed at a depth of 2.8 cm after deconvolution. The TA axial and lateral resolutions were ~0.5 and ~0.8 mm, respectively. In general, the spatial resolutions of this system are adequate for imaging clinically

significant breast tumors, which range in size from several millimeters to several centimeters.

3.2 PAT Penetration Depth in Chicken Breast Tissue

To measure the PAT penetration depth, an LDPE tube (7 mm inner diameter, 25 mm length) filled with oxygenated bovine blood was embedded in layers of chicken breast tissue. Chicken breast tissue has optical properties comparable to human breast tissue. The optical $1/e$ penetration depth in chicken breast tissue at 650 nm is between 0.9 and 1.6 cm,[32] and that of human breast tissue at 656 nm is about 0.78 cm.[33] During the experiment, the whole sample was placed inside a plastic container to support the layers of chicken breast tissue, as shown in Fig. 3(a). The same thicknesses of tissue were used above and below the tube to ensure that both the laser pulses and the generated acoustic signals traveled the same distance. With this arrangement, penetration-depth measurements acquired in transmission mode are analogous to reflection mode acquisitions, where both the source and detector are placed on the same side of the tissue. The laser beam had a diameter of ∼3.2 cm at the surface of the tissue, and the fluence was ∼19 mJ/cm². With these settings, a maximum penetration depth of 6.6 cm was obtained. Figure 3(b) shows a US image of the full sample captured on the US machine, when the blood tube boundary was 7.0 and 6.6 cm from the top and bottom surfaces, respectively. Figure 3(c) shows the corresponding overlaid PA/US image. PA signals from the blood at different depths were normalized to the signal at the smallest depth and are plotted in Fig. 3(d). By fitting the data according to the exponential decay, the $1/e$ penetration depth was calculated to be 0.84 cm, which was influenced by both laser and acoustic attenuations. The R^2 value of the fitting was 0.99. The 6.6-cm depth is approximately 7.9 times the $1/e$ penetration depth, corresponding to nearly 34 dB attenuation of the incident laser power density. The SNR at 6.6 cm in the reconstructed image was ∼24 dB.

The experiment was repeated using a tube filled with methylene blue solution (30 mM) as the target. The laser beam size

was 2.5 cm in diameter and the laser fluence was ∼17 mJ/cm². The maximum depth obtained was 8.4 cm, with an SNR of ∼15 dB. Figure 4(a) shows a photograph of the sample setup. Figure 4(b) and 4(c) shows the overlaid PA/US images at depths of 3.4 and 8.4 cm, respectively. To view the tube signal better, PA signals below a threshold value were suppressed, and only a small portion of the PA image containing the tube was shown, indicated by the dotted frame. PA signals at different depths were normalized to the signal at the smallest depth and are plotted in Fig. 4(d).

3.3 TAT Penetration Depth in Porcine Fat Tissue

A similar penetration-depth experiment for TAT was performed using porcine fat. The tube filled with 0.9% saline solution had an inner diameter of 13 mm and was 15 mm in length. This tube had comparable dimensions in all directions so that the polarity effect of the electric field was minimized. Figure 5(a) shows the tube embedded in layers of porcine fat. Figure 5(b) and 5(c) shows overlaid TA/US images at depths of 1.1 and 4.4 cm, respectively. Deconvolution was used to process the TA data. The maximum penetration depth obtained was 4.4 cm, where the SNR was ∼15.1 dB. Figure 5(d) shows the normalized TA signal in dB from the tube as a function of depth. Linear fitting of the measurement results gave an R^2 value of 0.99.

3.4 PAT Sensitivity for Methylene Blue

An LDPE tube was buried in layers of chicken breast tissue, positioned as shown in Fig. 6(a). The LDPE tube was tested to ensure that it was not stained by methylene blue during the experiment. The ends of the LDPE tube were cut open and connected to soft tygon tubes. Methylene blue solution of different concentrations was injected by syringe through the LDPE tube via the tygon tubes, without disrupting the sample position. The thicknesses of the chicken tissue above and below the tube were 3.5 and 3.4 cm, respectively. The laser fluence at the illuminated surface was 17 mJ/cm². First, the tube was filled with distilled water and the PA signal was recorded as a baseline. Next, methylene blue solution was injected into the tube at concentrations ranging from 2 μM to 1 mM. The baseline

Fig. 3 PA imaging of blood tube in chicken tissue. (a) Photograph showing the blood tube embedded in chicken breast tissue. The blood tube was covered by additional layers of chicken breast tissue during PA imaging. (b) US image of the whole sample when the depth is 6.6 cm. (c) PA and US overlaid image at 6.6 cm. (d) PA signal (normalized by the signal at the smallest depth) as a function of depth. The maximum depth is 6.6 cm. SNR at this depth is 16 (24 dB). The $1/e$ penetration-depth based on linear curve-fitting is 0.84 cm.
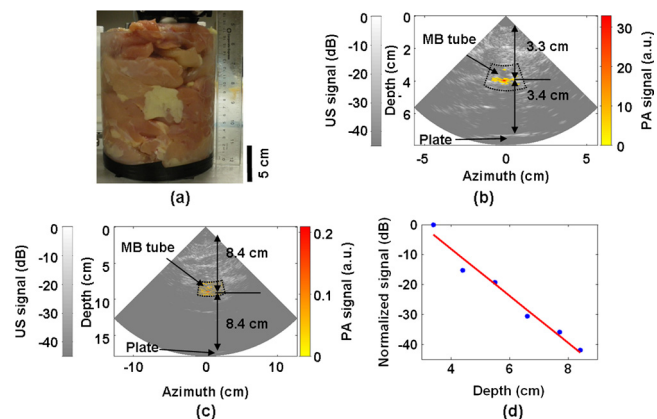

Fig. 4 PA imaging of a MB-containing tube in chicken tissue. MB, methylene blue. (a) Photograph of the sample setup. (b) Overlaid PA and US image of the tube at 3.4 cm depth. (c) Overlaid PA and US image of the tube at 8.4 cm depth. (d) PA signal (normalized by the signal at the smallest depth) as a function of depth. The maximum depth is 8.4 cm. SNR at this depth is 5.6 (15 dB). The $1/e$ penetration-depth based on linear curve-fitting is 1.11 cm.
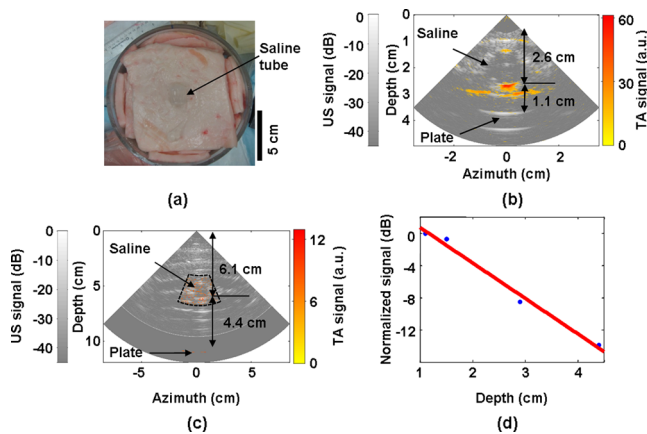
Fig. 5 TA imaging of saline tube in pork fat tissue. (a) Photograph showing the saline tube embedded in fat tissue. The saline tube was buried under additional layers of fat tissue during TA imaging. (b) TA and US overlaid image at a depth of 1.1 cm. (c) TA and US overlaid image of the tube at a depth of 4.4 cm (in the dotted frame). (d) TA signal (normalized by the signal at the smallest depth) as a function of depth. The maximum depth is 4.4 cm. SNR at this depth is 5.7 (15.1 dB).

PA signal, defined as the signal from the tube filled with water, was subtracted from the PA signal from each concentration of methylene blue. The contrast-to-noise ratio (CNR) in dB, defined as the ratio between the PA signal after background subtraction and the noise, is plotted in Fig. 6(b) versus the concentration of methylene blue on a log scale. The linear curve-fitting of these data gave an R^2 value of 0.996, which means the PA signal changed linearly as the concentration changed. At concentrations higher than 1 mM, the PA signal varied in a nonlinear fashion because of the depth-dependent distribution of optical energy deposition inside the methylene blue.[34] The SNR from the tube filled with 2 μM methylene blue was 7.8, or 17.8 dB. Therefore, the noise-equivalent sensitivity, defined as the ratio of the methylene blue concentration to the SNR, was ~260 nM at a depth of 3.4 cm in chicken breast tissue.

4 Discussion

We aimed to design a clinical imaging system that combines contrasts from PAT, TAT, and ultrasonography to monitor functional changes during breast neoadjuvant therapy and predict treatment efficacy. This new system is significantly different from previous systems[3,20] with respect to the ultrasound
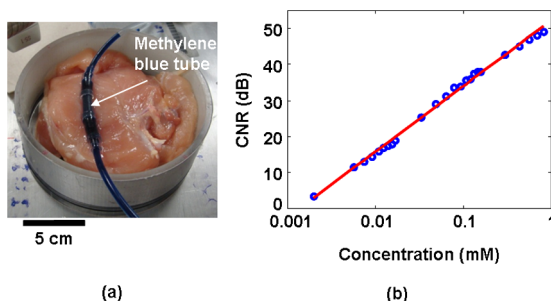
Fig. 6 PA signal strength as a function of methylene blue concentration at a depth of 3.4 cm measured using the S5-1 probe. (a) Photograph showing the methylene blue tube embedded in chicken breast tissue. The methylene blue tube was covered by 3.5 cm of chicken breast tissue during PA imaging. (b) CNR versus concentration after subtraction of the baseline signal.

detection system, light delivery scheme, and data acquisition. Both PAT and TAT work in transmission mode because of the size of the antenna. Moreover, decoupling the ultrasound transducer and laser/microwave source makes it possible to optimize the source path and the ultrasound path independently. PA and TA signals can be acquired in parallel, and PA, TA, and US data are exactly coregistered because they use the same array transducer for detection. With the free-space laser delivery design, we achieved a high laser fluence for PAT that was within ANSI safety limits.[35] The high laser fluence and probe sensitivity enabled PA imaging of blood at a depth of 6.6 cm in chicken breast tissue. We also imaged methylene blue at an even larger depth of 8.4 cm. This penetration depth exceeds the previously reported depth for PA detection of methylene blue by more than 3 cm, and the noise-equivalent sensitivity for methylene blue in chicken breast tissue measured with this system (260 nM at a depth of 3.4 cm) is a significant improvement over previous reports.[20]

The maximum penetration depth of our TAT combined with the clinical ultrasound system is 4.4 cm. The TA signal drop from 1 to 4 cm is much less than the PA signal drop for the same depth range. This suggests that the microwave attenuates more slowly than light in breast tissue, assuming the breast tissue has dielectric properties similar to porcine fat and optical properties similar to chicken tissue. The TAT system design can be improved to image more deeply by increasing the microwave energy.

We measured the resolution of the trimodality imaging system and found that it is suitable for deep PAT/TAT. These results help to quantify the system performance, which is critical for future clinical applications.

This study is not without limitations. We used chicken breast and porcine fat tissue to mimic human breast tissue; however, human breast tissue is more complicated. It consists of various structures and may contain more blood than excised chicken breast tissue and more water than porcine fat, thus attenuating more light and microwave energy. Breast tumors may be less absorptive than the methylene blue solution or salt water. The imaging penetration depth in real human breast tissue will be assessed more accurately in human subjects.

The interaction of microwave and biological tissues is rather complicated. The biological effects of microwaves do not depend solely on the external power density. The intensity of the internal fields depends on a number of parameters: frequency, intensity, and polarization of the external field; size, shape, and dielectric properties of the body; spatial configuration between the exposure source and the exposed body; and the presence of other objects in the vicinity.[36] In future clinical applications, improved image quality may be achieved by applying a compensation model during image reconstruction.

5 Conclusions

We developed a multimodality system that integrates three imaging techniques, namely, ultrasound, photoacoustic, and thermoacoustic tomography. The system adds PA and TA contrast mechanisms to traditional US imaging techniques and provides complementary information on optical, dielectric, and ultrasonic tissue properties. We evaluated the performance of the system in terms of penetration depth, spatial resolution, and sensitivity. Using endogenous hemoglobin contrast in whole blood, we demonstrated that the maximum penetration depth of PAT in chicken breast tissue was 6.6 cm; using

methylene blue solution, we showed that it was 8.4 cm. To our knowledge, this is the first time photoacoustic imaging at these depths has been reported. The maximum penetration depth of TAT in porcine fat was 4.4 cm. The noise equivalent sensitivity of the methylene blue solution in chicken tissue was measured to be 260 nM at a depth of 3.4 cm. These promising results motivate further development of the system for clinical applications in breast cancer imaging.

Acknowledgments

References

1. G. Ku et al., "Thermoacoustic and photoacoustic tomography of thick biological tissues toward breast imaging," *Technol. Cancer Res. Treat.* **4**, 559–565 (2005).
2. L. V. Wang, "Prospects of photoacoustic tomography," *Med. Phys.* **35**, 5758–5767 (2008).
3. M. Pramanik et al., "Design and evaluation of a novel breast cancer detection system combining both thermoacoustic (TA) and photoacoustic (PA) tomography," *Med. Phys.* **35**, 2218–2223 (2008).
4. R. A. Kruger, D. R. Reinecke, and G. A. Kruger, "Thermoacoustic computed tomography—technical considerations," *Med. Phys.* **26**, 1832–1837 (1999).
5. L. V. Wang et al., "Microwave-induced acoustic imaging of biological tissues," *Rev. Sci. Instrum.* **70**, 3744–3748 (1999).
6. M. Xu and L. V. Wang, "Photoacoustic imaging in biomedicine," *Rev. Sci. Instrum.* **77**, 041101 (2006).
7. Y. Xu and L. V. Wang, "Effects of acoustic heterogeneity on thermoacoustic tomography in the breast," *IEEE Trans. Ultrason. Ferroelectrics Freq. Contr.* **50**, 1134–1146 (2003).
8. R. A. Kruger et al., "Breast cancer in vivo: contrast enhancement with thermoacoustic CT at 434 MHz-feasibility study," *Radiology* **216**, 279–283 (2000).
9. R. A. Kruger et al. and R. P. Doyle, "Photoacoustic angiography of the breast," *Med. Phys.* **37**, 6096–6100 (2010).
10. S. Manohar et al., "Initial results of in vivo non-invasive cancer imaging in the human breast using near-infrared photoacoustics," *Opt. Express* **15**, 12277–12285 (2007).
11. S. A. Ermilov et al., "Laser optoacoustic imaging system for detection of breast cancer," *J. Biomed. Opt.* **14**, 024007 (2009).
12. X. D. Wang et al., "Noninvasive laser-induced photoacoustic tomography for structural and functional in vivo imaging of the brain," *Nat. Biotechnol.* **21**, 803–806 (2003).
13. G. Ku et al., "Imaging of tumor angiogenesis in rat brains *in vivo* by photoacoustic tomography," *Appl. Opt.* **44**, 770–775 (2005).
14. M. Pramanik, G. Ku, and L. V. Wang, "Tangential resolution improvement in thermoacoustic and photoacoustic tomography using a negative acoustic lens," *J. Biomed. Opt.* **14**, 024028 (2009).
15. H. Grün et al., "Three-dimensional photoacoustic imaging using fiber-based line detectors," *J. Biomed. Opt.* **15**, 021306 (2010).
16. M. Pramanik et al., "Single-walled carbon nanotubes as a multimodal-thermoacoustic and photoacoustic-contrast agent," *J. Biomed. Opt.* **14**, 034018 (2009).
17. L. Nie, Z. Guo, and L. V. Wang, "Photoacoustic tomography of monkey brain using virtual point ultrasonic transducers," *J. Biomed. Opt.* **16**, 076005 (2011).
18. S. Y. Emelianov et al., "Combined ultrasound, optoacoustic and elasticity imaging," *Proc. SPIE* **5320**, 101–112 (2004).
19. T. N. Erpelding et al., "Sentinel lymph nodes in the rat: noninvasive photoacoustic and US imaging with a clinical US system," *Radiology* **256**, 102–110 (2010).
20. C. Kim et al., "Deeply penetrating in vivo photoacoustic imaging using a clinical ultrasound array system," *Biomed. Opt. Express* **1**, 278–284 (2010).
21. C. Kim et al., "Handheld array-based photoacoustic probe for guiding needle biopsy of sentinel lymph nodes," *J. Biomed. Opt.* **15**, 046010 (2010).
22. D. R. Reinecke et al., "Co-registered photoacoustic, thermoacoustic and ultrasound mouse imaging," *Proc. SPIE* **7564**, 756420 (2010).
23. Q. Zhu et al., "Noninvasive monitoring of breast cancer during neoadjuvant chemotherapy using optical tomography with ultrasound localization," *Neoplasia* **10**, 1028–1040 (2008).
24. A. Cerussi et al., "Predicting response to breast cancer neoadjuvant chemotherapy using diffuse optical spectroscopy," *Proc. Natl. Acad. Sci. USA* **104**, 4014–4019 (2007).
25. IEEE International Committee on Electromagnetic Safety (SCC39), "IEEE Standard for Safety Levels with Respect to Human Exposure to Radio Frequency Electromagnetic Fields, 3 kHz to 300 GHz," *IEEE Std C95.1-2005 (Revision of IEEE Std C95.1-1991)*, pp. 1–238 (2006).
26. K. P. Köstli et al., "Temporal backward projection of optoacoustic pressure transients using Fourier transform methods," *Phys. Med. Biol.* **46**, 1863–1872 (2001).
27. K. R. Foster and J. L. Schepps, "Dielectric properties of tumor and normal tissues at radio through microwave frequencies," *J. Microw. Power* **16**, 107–119 (1981).
28. Y. Xu et al., "Reconstructions in limited-view thermoacoustic tomography," *Med. Phys.* **31**, 724–733 (2004).
29. X. Zeng, S. Yan, and G. Wang, "Effects of microwave pulse width on the spatial resolution of microwave-induced thermoacoustic imaging," *Antennas, Propagation & EM Theory, 2006. ISAPE '06. 7th International Symposium on*, pp. 1–4 (2006).
30. G. Ku and L. V. Wang, "Scanning microwave-induced thermoacoustic tomography: signal, resolution, and contrast," *Med. Phys.* **28**, 4–10 (2001).
31. M. J. E. Salami and S. N. Sidek, "Performance evaluation of the deconvolution techniques used in analyzing multicomponent transient signals," *TENCON 2000, Proc.* **1**, 487–492 (2000).
32. G. Marquez et al., "Anisotropy in the absorption and scattering spectra of chicken breast tissue," *Appl. Opt.* **37**, 798–805 (1998).
33. L. Spinelli et al., "Bulk optical properties and tissue components in the female breast from multiwavelength time-resolved optical mammography," *J. Biomed. Opt.* **9**, 1137–1142 (2004).
34. M. Sivaramakrishnan et al., "Limitations of quantitative photoacoustic measurements of blood oxygenation in small vessels," *Phys. Med. Biol.* **52**, 1349–1361 (2007).
35. American National Standards Institute, *American National Standard for Safe Use of Lasers ANSI Z136.1-2000*, Laser Institute of America (2000), ISBN: 978-0-912035-65-9.
36. A. Vorst, A. Rosen, and Y. Kotsuka, *RF/Microwave Interaction with Biological Tissues*, IEEE Press, Totowa, NJ (2006).